ELSEVIER
Available online at www.sciencedirect.com
SCIENCE DIRECT®
Ocean Modelling xxx (2003) xxx–xxx
Ocean Modelling
www.elsevier.com/locate/omodol

Grid geometry effects on convection in ocean climate models: a conceptual study

Sven Titz [a,*], Till Kuhlbrodt [b], Ulrike Feudel [c]

[a] *Institute for Physics, University of Potsdam, PF 601553, 14415 Potsdam, Germany*
[b] *Potsdam Institute for Climate Impact Research, PF 60 12 03, 14412 Potsdam, Germany*
[c] *Institute for Chemistry and Biology of the Marine Environment, PF 2503, 26111, Oldenburg, Germany*

Received 7 February 2003; received in revised form 14 July 2003; accepted 12 August 2003

Abstract

Ocean convection is a highly non-linear and local process. Typically, a small-scale phenomenon of this kind entails numerical problems in the modelling of ocean circulation. One of the tasks to solve is the improvement of convection parameterization schemes, but the question of grid geometry also plays a considerable role. Here, this question is studied in the context of global ocean models coupled to an atmosphere model. Such ocean climate models have mostly structured, coarsely resolved grids.

Using a simple conceptual two-layer model, we compare the discretization effects of a rectangular grid with those of a grid with hexagonal grid cells, focussing on average properties of the ocean. It turns out that systematic errors tend to be clearly smaller with the hexagonal grid. In a hysteresis experiment with the atmospheric boundary condition as a hysteresis parameter, the spatially averaged behaviour shows non-negligible artificial steps for quadratic grid cells. This bias is reduced with the hexagonal grid. The same holds for the directional sensitivity (or horizontal anisotropy) which is found for different angles of the advection velocity. The grid with hexagonal grid cells shows much more isotropic results. From the limited viewpoint of these test experiments, it seems that the hexagonal grid (i.e. icosahedral–hexagonal grids on the sphere) is recommendable for ocean climate models.

Keywords: Oceanic convection; Ocean modelling; Parameterization; Model grid

* Corresponding author.
E-mail address: sven@agnld.uni-potsdam.de (S. Titz).

1463-5003/$ - see front matter © 2003 Published by Elsevier Ltd.
doi:10.1016/j.ocemod.2003.08.001

1. Introduction

To the largest part of its extent, the world ocean is stratified in a statically stable way, so that vertical exchange processes are weak. Only in a few small regions in the North Atlantic, the Mediterranean, and the Southern Ocean, a combination of wind stress forcing, freshwater advection and surface heat fluxes may succeed in diminishing this stratification. In places where the vertical density gradient actually vanishes, one observes a strong vertical turbulent mixing to depths of 2 km and more. This process, occurring only for a few days at a time, and on spatial scales of only $\sim$50 km, is called deep convection (see Marshall and Schott (1999) for a comprehensive review).

Convection constitutes a much more efficient vertical heat transfer process than vertical (diapycnal) mixing. Therefore it is essential for ocean general circulation models that both location and timing of convection are captured. Furthermore, convection events are a crucial part of the overturning circulation in the North Atlantic that ensures today's climatic conditions in the North Atlantic region. But the small spatial and temporal scales of convection prevent a direct representation in global ocean models that are part of a climate model (called ocean climate models here) as their resolution is too coarse. Hence, in ocean climate models, convection is parameterized. Convective adjustment (Cox, 1984; Rahmstorf, 1993) and an increased vertical diffusion coefficient in places where the stratification is weak (Klinger et al., 1996; Molemaker and Dijkstra, 2000) are the most commonly used parameterization schemes. Convection parameterizations have been studied thoroughly, but the role of the model grid geometry has been considered much less.

In ocean models that are not coupled to a dynamical atmosphere, unstructured grids are often used. They can be adapted to a given orography in a very efficient way. On the other hand, the coupling to an atmospheric component with its structured grid is rather complicated. This is a major disadvantage of unstructured ocean model grids for their application in efficiently coupled climate models (Randall et al., 2002). In their review of ocean climate modelling, Griffies et al. (2000) mention two other problems of unstructured grids: the difficulty to represent the correct geostrophic balance, and unphysical wave scattering due to grid space variation. Griffies et al. (2000) state that in most ocean climate models structured grids are implemented. Very often, generalized orthogonal coordinates are used, which means that the pole problem can be avoided by shifting the grid pole to the centre of a land mass. Structured grids without orthogonal coordinates exist, too: grids with triagonal and with hexagonal grid cells. The latter are called icosahedral–hexagonal on the sphere (where some few pentagonal grid cells have to be included). Very recently, these grids have been tested by atmosphere modellers (Ringler et al., 2000; Majewski et al., 2000; Tomita et al., submitted). The results are similar to those obtained with spherical orthogonal coordinates (often used in atmosphere models), but the theoretical projection of computation times looks definitely better for icosahedral–hexagonal grids. This is one of the reasons why Randall et al. (2002) recommend these grids for climate modelling, both for atmosphere models and for ocean models.

In this paper, we investigate how the grid geometry influences the spreading of convection, i.e. the spatial enlargement of convective regions, in ocean climate models. For this purpose, we use a simplified two-layer model with a conceptual representation of ocean dynamics and compare the features of rectangular grids with those of a grid with hexagonal grid cells (i.e. icosahedral–hexagonal grids on the sphere).

Hecht et al. (2000) state in favour of such conceptual experiments that the ''evaluation of schemes may be facilitated through the consideration of simpler [...] test problems, designed to challenge the performance of algorithms in fundamental, important ways.'' In Hecht et al. (2000), a new test problem for ocean tracer transport is presented. The rotation of the grid by 45° is the essential test ingredient. The authors find a sensitivity to the orientation of the model grid. In our paper, we also address the question of horizontal (an)isotropy.

The interaction between the convective adjustment scheme and horizontal eddy diffusion has been studied in a conceptual way by Cessi and Young (1996). They show that there is a strong sensitivity to initial conditions and that simulation runs with similar initial conditions can lead to solutions with very different average properties. In Cessi (1996) an instability on the grid scale is described. The instability is caused by the convective adjustment scheme.

The paper is organized as follows: it starts in Section 2 with the description of the two-layer ocean model used for our investigation. Section 3 is devoted to numerical experiments in which the spatially averaged effect of grid geometry is examined. This is done by using the atmospheric boundary condition for heat flux as a hysteresis parameter. The sensitivity to the direction of advection is studied in Section 4. For this purpose, a homogeneous advective field is added to the equations. Section 5 contains results with a hexagonal grid for both test experiments (hysteresis and directional sensitivity). The effect of isopycnal mixing is investigated in Section 6. Conclusions are given in Section 7.

2. Description of the model with square grid cells

We study the mechanisms of discretization effects that occur when convection spreads in ocean climate models. By *spreading of convection* we mean the spatial enlargement of an area of convective grid cells. To address general features of the problem, the model we use is strongly simplified. Nevertheless, it captures convective mixing and eddy-diffusion; including advection is an additional option. Since the local, parameterized convection process and its modification by horizontal coupling through eddy-diffusion (and advection) is the focus of our interest, we use the temperature and the salinity as prognostic variables and neglect the momentum budget. The model possesses two vertical layers, and its horizontal scale is of the same magnitude as the basin scale. It has a horizontal grid resolution of $\Delta x = 250$ km and 16×16 grid points. We assume that the volume of the lower grid point is twice the volume of the upper one. This ratio mimics the increasing layer thickness (with increasing depth) in ocean models. The dynamics at the grid points is determined by convective mixing (achieved through convective adjustment: CA) and lateral eddy-diffusive mixing D. In the upper layer, surface fluxes (freshwater and heat) and optional advection A (described in Section 4) are added. Omitting the horizontal indices, the prognostic equations read

$$\frac{\partial}{\partial t} T^{(1)} = \frac{1}{\tau_\mathrm{r}} (T_\mathrm{r} - T^{(1)}) + D_{T^{(1)}} \quad \{+A_{T^{(1)}}\} \quad [+\mathrm{CA}] \tag{1}$$

$$\frac{\partial}{\partial t} S^{(1)} = F_\mathrm{salt} + D_{S^{(1)}} \quad \{+A_{S^{(1)}}\} \quad [+\mathrm{CA}] \tag{2}$$

$$\frac{\partial}{\partial t} T^{(2)} = D_{T^{(2)}} \quad [+\mathrm{CA}] \tag{3}$$

$$\frac{\partial}{\partial t} S^{(2)} = D_{S^{(2)}} \quad [+\mathrm{CA}] \tag{4}$$

$T^{(1)}$ and $S^{(1)}$ are the temperature and salinity of an upper grid point at time t, while $T^{(2)}$ and $S^{(2)}$ represent the respective lower grid point. For the surface fluxes, we use mixed boundary conditions: a constant freshwater flux F_{salt} in combination with the temperature of the upper grid point being relaxed towards a restoring temperature T_{r}. Mixed boundary conditions are widely used to represent the thermally strong coupling between the ocean surface layer and the atmosphere, while a similar salinity feedback is absent. For the freshwater flux F_{salt}, we use the estimate -1×10^{-4} psu d^{-1}. Thus, the surface layer is slowly freshened which corresponds to climatic conditions at high latitudes (where precipitation exceeds evaporation). The temperature restoring timescale τ_{r} is chosen to be five months. This timescale can be derived from observational data, see Kuhlbrodt et al. (2001). A Euler forward scheme with a time step Δt of one day is applied. After each iteration, a simple *convective adjustment* (CA) scheme is carried out: if the vertical density difference $\rho_1 - \rho_2$ becomes zero or larger, the two grid cells will be mixed completely. Here, a linear approximation of the density equation is used

$$\rho(T, S) = \rho_0(1 + \beta(S - S_0) - \alpha(T - T_0)) \tag{5}$$

The index 0 denotes reference values (that are irrelevant here, since we only use the density difference); α and β are the expansion coefficients for temperature and salinity. We use the values $\alpha = 0.00017\ \mathrm{K}^{-1}$ and $\beta = 0.0008\ \mathrm{psu}^{-1}$. Since the volume of the lower cell is twice the volume of the upper one, the final mixed temperature of the two cells reads in its discretized form

$$T^{\mathrm{mix}}_{t+\Delta t} = \frac{T^{(1)}_{t+\Delta t} + 2T^{(2)}_{t+\Delta t}}{3} \tag{6}$$

The local grid cells are coupled horizontally through eddy-diffusion (in Section 4, an advective field A is added). Horizontal coordinate indices are i and j; they refer to longitude and latitude, respectively. The diffusion term $D_{T^{(1)}}$ reads

$$\begin{aligned} D_{T^{(1)}} &= \kappa_{\mathrm{h}} \nabla^2_{\mathrm{h}} T^{(1)} \\ &\approx \frac{\kappa_{\mathrm{h}}}{(\Delta x)^2}\left(T^{(1)}(i-1,j) + T^{(1)}(i,j-1) + T^{(1)}(i+1,j) + T^{(1)}(i,j+1) - 4T^{(1)}(i,j)\right) \end{aligned} \tag{7}$$

The eddy-diffusion constant κ_{h} is set to $3.0 \times 10^3\ \mathrm{m}^2\,\mathrm{s}^{-1}$ which is a typical value for ocean climate models of coarse resolution (Braconnot et al., 1997). The parameter values of the model are shown in Table 1. *No flux* boundary conditions are applied.

Laplacian diffusion is used here which is one of the simplest eddy diffusion schemes. Today higher order schemes (like biharmonic diffusion) are applied more and more often in ocean models. Therefore, one may ask why they are not taken into account in this study. But concerning the efficiency of coupled climate models, higher order schemes have two disadvantages: high CPU costs and unphysical long-range coupling. The computation time required for biharmonic diffusion is increased by the fact that this scheme is not positive-definite and therefore needs a correction term. Every eddy diffusion parameterization has the drawback of unphysical long-range

Table 1
Parameter values of the conceptual two-layer model

Parameter	Denotation	Value
Grid resolution	Δx	250 km
Time step	Δt	1 day
Restoring time scale	τ_r	5 months
Salt flux	F_{salt}	-1×10^{-4} psu d^{-1}
Eddy diffusion constant	κ_h	3×10^{3} $m^2\,s^{-1}$

coupling, but if only direct neighbours are taken into account, this drawback will be minimized. Hence we apply the Laplacian diffusion scheme here and discuss whether another grid geometry (namely hexagonal grid-cells) can reduce the discretization effects.

The ocean can be in a state of bistability with respect to convection, which has been shown by Lenderink and Haarsma (1994) in simple ocean general circulation models and by Kuhlbrodt et al. (2001) in conceptual box models. By contrast, here we are rather interested in the transient behaviour during one period of convection. Hence, with our model, we do not perform long simulations with constant parameters (maximum integration time: 160 days), and we do not distinguish between two stable states but between two different local *transients*: one that is permanently convective (CA at every time step) and another one that is initially non-convectivc but may become convective during the simulation. The onset of convection is characterized by a jump of the values of the variables.

3. Average behaviour: hysteresis curves with artificial steps

The first effect to be studied is the *average* behaviour of an area in the ocean model with convective and non-convective grid points, when temporarily strong buoyancy forcing prevails at the surface. Thus, a transition of non-convective elements to convection is favoured. We use two alternative types of initial conditions (IC) for each pair (i,j) of horizontal coordinates—convective IC and non-convective IC

$$T^{(1)}_{\mathrm{con}} = T^{(2)}_{\mathrm{con}} = 4\ {}^\circ\mathrm{C} \tag{8}$$

$$S^{(1)}_{\mathrm{con}} = S^{(2)}_{\mathrm{con}} = 35\ \mathrm{psu} \tag{9}$$

$$T^{(1)}_{\mathrm{non}} = 0\ {}^\circ\mathrm{C} \tag{10}$$

$$S^{(1)}_{\mathrm{non}} = 33.7\ \mathrm{psu} \tag{11}$$

$$T^{(2)}_{\mathrm{non}} = 4\ {}^\circ\mathrm{C} \tag{12}$$

$$S^{(2)}_{\mathrm{non}} = 35\ \mathrm{psu} \tag{13}$$

The IC are randomly distributed with the ratio

$$R_0 = \frac{n_{0,\mathrm{con}}}{n_{0,\mathrm{non}} + n_{0,\mathrm{con}}}$$

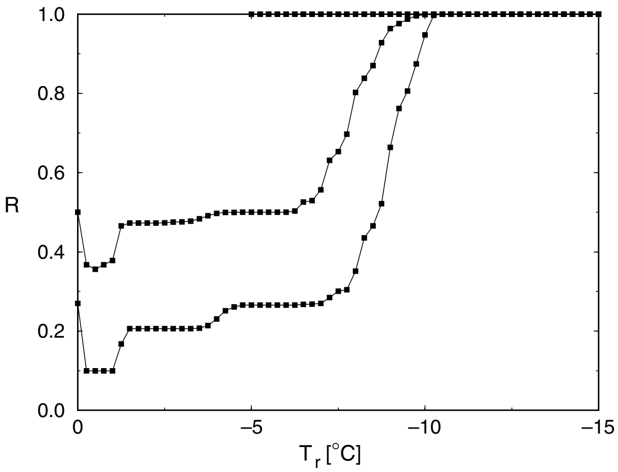

Fig. 1. Hysteresis curves for $R_0 = 0.5$ (upper curve) and $R_0 \approx 0.27$ (lower curve). The restoring temperature T_r is the hysteresis parameter. We average over 200 realizations with randomly distributed initial conditions (but fixed R_0).

between the number of convective and all grid cells. The hysteresis run consists in a stepwise decrease and increase of the surface restoring temperature T_r. After two time steps, T_r is changed by 0.25 °C. We use a time step of one day. The hysteresis curve starts at $T_r = 0$ °C, turns at $T_r = -15$ °C, and ends at $T_r = -5$ °C. We average over 200 realizations of the hysteresis run.

In Fig. 1, the ratio R between convective and all grid cells is shown depending on the restoring temperature T_r. Two hysteresis curves for different initial ratios R_0 are presented: one for $R_0 = 0.5$ and one for $R_0 \approx 0.27$ (68 convective elements). In both cases, the curve jumps to a value $R < R_0$ within one step of the hysteresis parameter, because of single convective elements that have only non-convective neighbours do not remain convective after the first time step with the initial R_0 chosen. Convection is suppressed by eddy-diffusive transport from neighbour grid cells. Naturally, this effect is larger for $R_0 \approx 0.27$, since the probability of convective elements having no convective neighbour is larger. The decrease of the restoring temperature does not lead to a continuous increase of R, but the increase occurs stepwise. In both cases ($R_0 = 0.5$ and $R_0 \approx 0.27$), two steps to the left of the steep slope at −8 °C can be distinguished. At lower restoring temperatures (around −8 °C), R quickly approaches the value 1 in both curves of Fig. 1, and $R = 1$ remains until the restoring temperature reaches −15 °C where the direction of restoring temperature change is reversed. The system remains in a totally convective state, while the restoring temperatures are increasing again. Hence, the system exhibits hysteretic behaviour. The hysteresis curves end at $T_r = -5$ °C, since we do not want to study the transition back to non-convective conditions here.

The steps between $T_r = -0.5$ °C and $T_r = -2$ °C and between $T_r = -2$ °C and $T_r = 5$ °C indicate that *discretization effects* are at work. They are caused by thresholds of local patterns in the model grid. This effect is similar to the one described by Vellinga (1998) who attributed the multistability of a model ocean to a CA-related local bistability. The latter gives rise to a finite number of thresholds at which single grid points switch between the non-convective and the

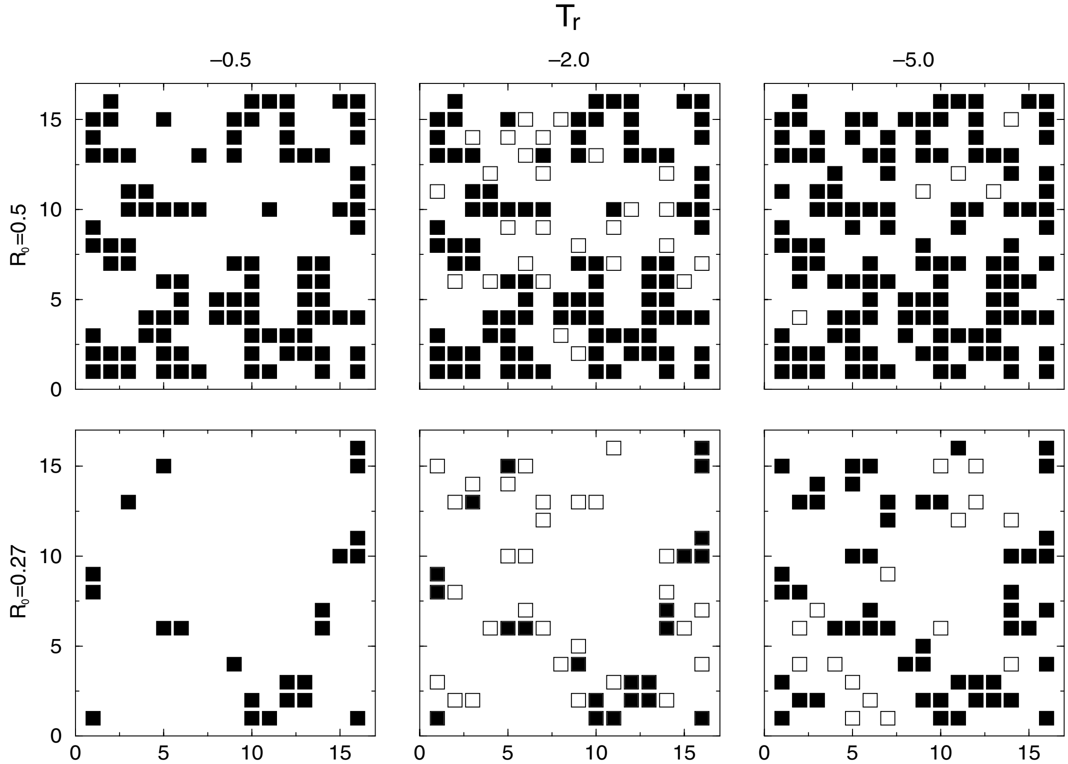

Fig. 2. Thresholds of small patterns determine hysteresis steps. Snapshots of two single realizations during the hysteresis run are shown here. Upper row: $R_0 = 0.5$ for $T_r = -0.5$ °C (left), $T_r = -2$ °C (centre), and $T_r = -5$ °C (right). Lower row: $R_0 \approx 0.27$ for $T_r = -0.5$ °C, $T_r = -2$ °C, and $T_r = -5$ °C. Convective grid points are represented as filled squares; new convective grid points (in comparison with the respective figure to the left) as empty squares.

convective state. In Fig. 2, the distribution of convective grid points before and after the major steps is shown; black squares denote convection. In our case, even for *averaged* hysteresis curves with *randomly* distributed IC, the discretization effect is visible: the hysteresis curves exhibit a staircase-like behaviour. Thus, it cannot be argued that weather fluctuations of the atmosphere or the ocean would cause discretization effects in ocean climate models to disappear (“average them out”). By contrast, discretization effects might lead to *systematic errors* on the average.

If one takes a closer look at the change of the convective patterns in Fig. 2, one will see that the two jumps of the hysteresis curves in Fig. 1 refer to two different transitions

(1) At $T_r = -2$ °C, *direct* neighbours of convective cells and some grid point pairs within non-convective areas have become convective. Thus, a threshold for direct neighbours of convective grid points has been overcome. The grid point pairs become convective because they initially (at $T = 0$ °C) had a convective IC but non-convective neighbours, suppressing convection during the first steps of the hysteresis curve. When T_r is decreased, switching to convection becomes possible. The same holds for some few switching grid points at the grid boundary. Possibly these three small pattern switches are not fully identical, but together they obviously make up the step in the hysteresis curve.
(2) At $T_r = -5$ °C, the new convective grid points correspond to a *checkerboard* pattern that can sometimes be found in ocean climate models. In this pattern, the convectivc (and non-convective) grid points are distributed like the black (or white) fields on a checkerboard.

Based on a statistical analysis, the two patterns responsible for the two steps can be distinguished. First, we define the number N_{dir} of direct, convective neighbours of a grid cell that has just become convective. Numerically, it is found for arbitrarily many realizations that

$$N_{dir}(T_r = -2\ ^\circ\mathrm{C}) = 1 \quad N_{dir}(T_r = -5\ ^\circ\mathrm{C}) = 0$$

hold for both initial ratios R_0 and every new convective grid cell. The step between $T_r = -0.5$ °C and $T_r = -2$ °C is related to additional convection in grid cells with exactly one convective neighbour cell. But this result does not yet tell anything about the pattern responsible for the second step. In order to find out whether a *checkerboard* pattern can be discovered, every grid cell with the indices $(i \pm 2, j)$, $(i, j \pm 2)$, or $(i \pm 1, j \pm 1)$ is defined as one of the eight checkerboard neighbours of the grid cell with the indices (i, j). The definition is illustrated in Fig. 4.

Fig. 3 shows probability distributions of the number N_{chess} of convective checkerboard neighbours for the two initial ratios R_0. In the case $R_0 = 0.5$, the majority of newly convecting cells has 4 or more convective checkerboard neighbours. In the case $R_0 \approx 0.27$ however, about 8% of the new convective grid cells have no convective checkerboard neighbour. We conclude that the checkerboard pattern becomes the more important the more convective cells already exist. Boundary grid cells are excluded from the analysis of the patterns.

The mechanism of the described discretization effect can be studied and explained with even simpler models: in Lind et al. (accepted) and Titz (2002), a lattice of coupled bistable maps was used in order to study phenomena like the staircase shape of hysteresis curves (and the sensitivity of advection which we show in the next section). It turned out that such discretization effects can be described by a local bistability that is represented by one prognostic equation and the respective diffusive coupling operator.

4. Sensitivity to the direction of advection

Advection plays an important role during the development of a convective area in the ocean. But in the context of our study it may *hide* certain discretization effects if geostrophic adjustment is incorporated in the model. Here we investigate whether there might exist a significant sensitivity to the direction of advection. Therefore a *homogeneous*, unidirectional advective field is added to our model equations. In other words, the advantage of conceptual clarity is paid for with a less

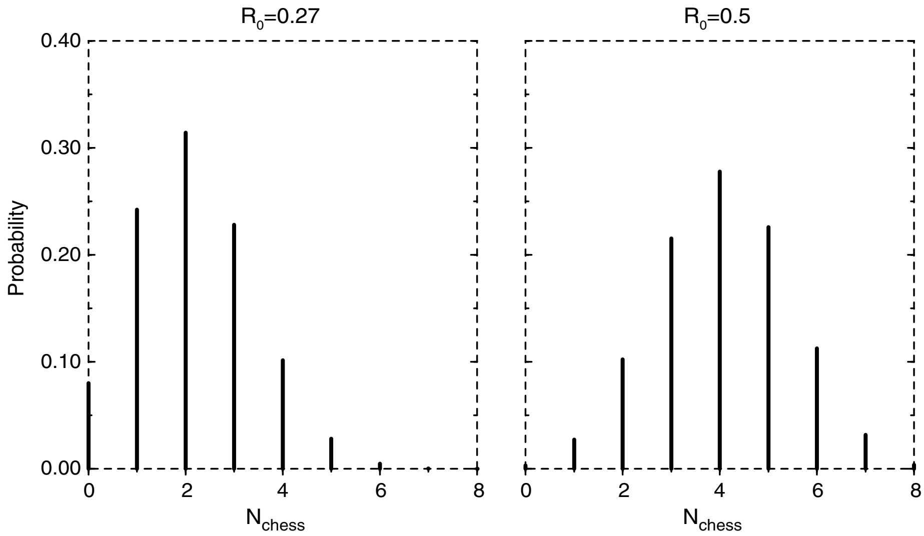

Fig. 3. Probability distributions of the number of convective checkerboard neighbours that a new convective grid cell will have. This figure refers to the step on the hysteresis curve between $T_r = -2$ °C and $T_r = -5$ °C. 500 000 realizations are used.

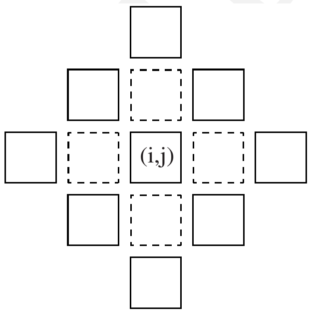

Fig. 4. The checkerboard neighbour cells of the cell (i, j) are depicted as solid squares.

realistic velocity field. The prognostic equations of the surface variables are extended by an advective term A. For discretization, the centered differences scheme is used

$$\begin{aligned} A_{T^{(1)}} &= \mathbf{v}_\mathrm{h} \cdot \nabla_\mathrm{h} T^{(1)} \\ &\approx \frac{1}{2} u(T^{(1)}(i-1,j) - T^{(1)}(i+1,j)) + \frac{1}{2} v\big(T^{(1)}(i,j-1) - T^{(1)}(i,j+1)\big) \end{aligned} \tag{14}$$

The horizontal coordinates u and v of the velocity vector correspond to the polar coordinates θ and $|\mathbf{v}|$, the angle and the amplitude of the advective velocity vector

$$\begin{aligned} u &= |\mathbf{v}| \cos\theta \\ v &= |\mathbf{v}| \sin\theta \end{aligned}$$

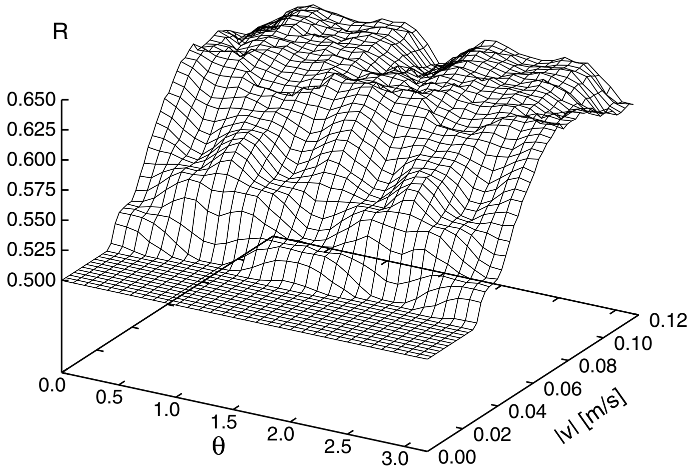

Fig. 5. Sensitivity to the direction of advection. The atmospheric restoring temperature T_r is set to be −5 °C. θ is the angle of the advective velocity and $|\mathbf{v}|$ its amplitude. R is the average value of 200 realizatons with randomly distributed I's.

As in the hysteresis experiments, we use *no flux* boundary conditions for the diffusion. The boundary condition for the advection term of a boundary element ($i = 1, 2 \leqslant j \leqslant 15$) reads

$$A_{T^{(1)},\text{boundary}} \approx \frac{1}{2}u(\underline{T^{(1)}(i,j)} - T^{(1)}(i+1,j)) + \frac{1}{2}v(T^{(1)}(i,j-1) - T^{(1)}(i,j+1)) \tag{15}$$

Thus, the quantity advected from the boundary (underlined) is set to be identical to the element (i, j), so that the boundaries do not influence the dynamics via advection.

For a ratio $R_0 = 0.5$ and a realistic range of the angle and the amplitude of the advective velocity, the ratio R after 40 days is simulated. 200 realizations of the experiment are done. The average result is shown in Fig. 5. When $|\mathbf{v}|$ has crossed a threshold, the convective area may become larger. The final ratio R does not only depend on the amplitude of the advective velocity but also on its angle θ. This double dependence is obvious in Fig. 6 that displays the contour lines of R. Differences in the final value of R for the same $|\mathbf{v}|$ can amount to up to 10%. Previously, this kind of horizontal anisotropy was found e.g. by Hecht et al. (2000) who studied advection schemes with rotated grid orientation. They found that a standard wind-driven gyre as a test case is simulated differently with the grid tilted by 45 °C. In addition, our results indicate that local bistability increases the anisotropic effect strongly.

5. Hexagonal grid cells versus square grid cells

Model grids with hexagonal grid cells (Fig. 7) have been used for the first time by atmosphere modellers (Sadourny et al., 1968; Williamson, 1968). The sphere can be covered with hexagons and a few pentagons in a very homogeneous way (Baumgardner and Frederickson, 1985; Tomita et al., 2002), avoiding the pole problem, while in the plane, hexagons can be used exclusively. Together with triangles and squares, hexagons are the only regular polygons that can tile a plane,

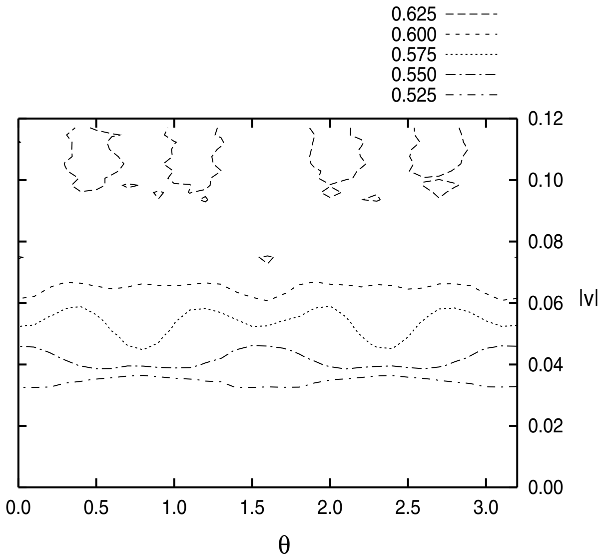

Fig. 6. Contour plot of the sensitive dependence of R on θ and $|\mathbf{v}|$ in Fig. 5. The angle θ for which R has a maximum is not fixed but depends itself on $|\mathbf{v}|$.

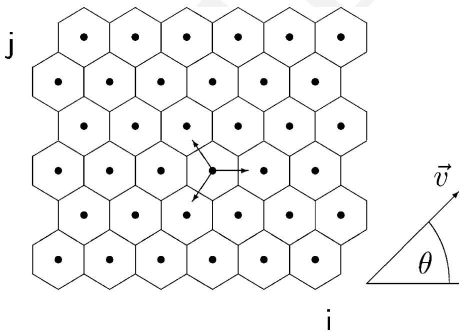

Fig. 7. Sketch of a grid with hexagonal grid cells. Each grid cell has six neighbour cells. On the right hand side, the velocity vector $\vec{v}$ and the corresponding advection angle θ are shown. They are used in the advection experiments of Section 5.2.

and hexagons have the highest symmetry of the three polygons. This guarantees a good horizontal isotropy, which manifests itself in good test results concerning wave propagation. Equivalents to the common staggered difference grids (Arakawa grids) exist on hexagonal grids; see for example Popović et al. (1996). Icosahedral grids have been tested with the shallow-water equations (Heikes and Randall, 1995a,b; Thuburn, 1997; Tomita et al., 2001; Ringler and Randall, 2002) and with the atmospheric general circulation (Ringler et al., 2000; Majewski et al., 2000; Tomita et al., submitted). The propagation of quasi-geostrophic modes was studied analytically on several difference grids (Popović et al., 1996). Ničković et al. (2002) investigated the geostrophic adjustment process on selected hexagonal grids with a simple two-dimensional linearized model of the atmosphere.

In this section of the paper, we show that the good horizontal isotropy and the larger number of direct local neighbour grid cells (six instead of four) can improve the model behaviour. Especially for coupled ocean-atmosphere climate models, hexagonal grid cells may be a useful alternative to square grids. Randall et al. (2002) propose that a icosahedral–hexagonal grid could be used for both the ocean model and the atmosphere model, and in coastal areas, hexagonal grids could be additionally refined, in a similar way as rectangular grids.

In the following, the previous experiments are repeated on the hexagonal grid and compared with those on the square grid. The same distance between neighbouring grid points is used, so that the area covered by the hexagonal grid is 13% smaller.

5.1. Hysteresis curves with hexagonal grid cells

The hysteresis experiments are repeated on the hexagonal grid. Again, *no flux* lateral boundary conditions are used. The discretized eddy-diffusion term is adapted to the grid geometry

$$\begin{aligned} D_{T^{(1)}} &= \kappa_\mathrm{h} \nabla_\mathrm{h}^2 T^{(1)} \\ &\approx \frac{2\kappa_\mathrm{h}}{3(\Delta x)^2} \big(T^{(1)}(i-1,j) + T^{(1)}(i,j-1) + T^{(1)}(i+1,j) + T^{(1)}(i,j+1) \\ &\quad + T^{(1)}(i \pm 1, j-1) + T^{(1)}(i \pm 1, j+1) - 6T^{(1)}(i,j)\big) \end{aligned} \tag{16}$$

The sign of the fifth and sixth right-hand side term alternates depending on j (see Fig. 7).

In Fig. 8, the hysteresis curves for the hexagonal grid are compared with the previous result (Fig. 1). The two curves look almost the same, except for small T_r-values. We have already mentioned that the difference between R_0 and R at the starting point of the hysteresis curves is caused by ‘‘disappearing’’ isolated convective elements. In the hexagonal grid, some of those elements ‘‘survive’’. Since every grid cell has six neighbours instead of four, there are more possibilities how convective and non-convective grid cells are arranged in patterns. The probability of having a convective neighbour cell is larger, increasing the number of ‘‘surviving’’ convective cells. In contrast to the square grid, there is no step at $T_\mathrm{r} = -2$ °C.

Since the hysteresis curve performed with the hexagonal grid exhibits smaller steps, this grid seems to behave in a smoother way with respect to the spreading of convective cells.

5.2. Less anisotropy with hexagonal grid cells

Now the sensitivity to the direction of the advective velocity is examined. For the implementation of advection on the hexagonal grid, a discretized advection term is necessary. Three instead of two horizontal velocity vector components are used now (see Fig. 7). The velocity components are expressed by means of the square grid's velocity amplitude $|\mathbf{v}|$

$$v_{0^\circ} = \sqrt{\frac{2}{3}}|\mathbf{v}|\cos\theta \tag{17}$$

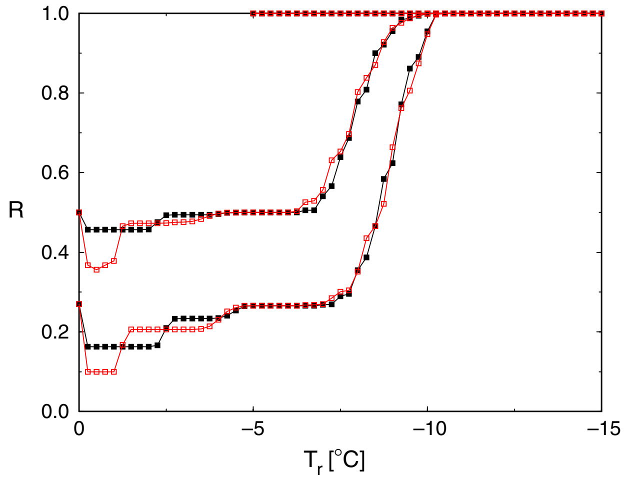

Fig. 8. Hysteresis curves for $R_0 = 0.5$ (upper curves) and $R_0 \approx 0.27$ (lower curves). (Filled squares) Hexagonal grid and (empty squares) square grid.

$$v_{120^\circ} = \sqrt{\frac{2}{3}}|\mathbf{v}|\cos(\theta + 120^\circ) \tag{18}$$

$$v_{240^\circ} = \sqrt{\frac{2}{3}}|\mathbf{v}|\sin(\theta - 30^\circ) \tag{19}$$

Thus, the advective term for the surface temperature $T^{(1)}$ reads

$$\begin{aligned} A_{T^{(1)}} = {} & \frac{1}{2}v_{0^\circ}(T^{(1)}(i,j,\mathrm{up},0^\circ) - T^{(1)}(i,j,\mathrm{down},0^\circ)) + \frac{1}{2}v_{120^\circ}(T^{(1)}(i,j,\mathrm{up},120^\circ) \\ & - T^{(1)}(i,j,\mathrm{down},120^\circ)) + \frac{1}{2}v_{240^\circ}(T^{(1)}(i,j,\mathrm{up},240^\circ) - T^{(1)}(i,j,\mathrm{down},240^\circ)) \end{aligned} \tag{20}$$

where the indices "up" and "down" refer to the upstream and downstream values of temperature in the grid (see Fig. 7).

When the experiment with advection is repeated on the hexagonal grid, less sensitivity to the direction of the advective velocity is found (see Fig. 9). Nevertheless, the general behaviour remains the same. The different symmetry properties of the hexagonal grid are clearly visible (three maxima instead of two).

The hexagonal grid is preferable because its horizontal isotropy is clearly better than the behaviour of the square grid. A similar effect would be caused by taking into account more neighbour grid cells on the square grid, but this is computationally much more expensive. Note that the hexagonal grid has more grid points per unit area (for the same horizontal distance between neighbouring grid points) and that the isotropy-reducing effect still works with a lower resolution and a computation time that is equivalent to the square grid.

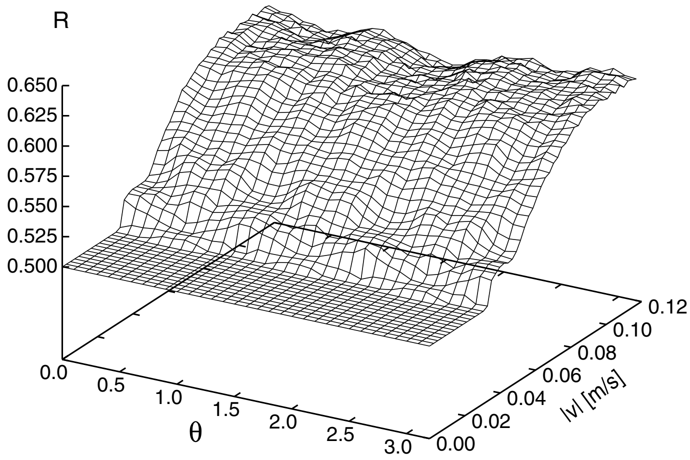

Fig. 9. Less sensitivity to the direction of advection on the hexagonal grid. θ is the angle of the advective velocity and $|\mathbf{v}|$ its amplitude. Compare this figure with Fig. 5.

6. The effect of isopycnal mixing

During the last years, purely horizontal tracer mixing has been replaced more and more by schemes like the GM scheme (Gent and McWilliams, 1990) that take isopycnal mixing into consideration. It turned out that isopycnal mixing may be a useful (although not fully convincing) alternative with regard to the occurrence of deep convection events. Therefore, we repeat our hysteresis experiments (without advection, see Section 3) with a simplified isopycnal mixing scheme: if CA has taken place at a certain grid point, the subsequent eddy-diffusion of the *surface* layer at this grid point is performed with the surrounding grid points in the *lower* layer that always have approximately the same density as surface grid points after convective mixing. There are no other diffusive fluxes. This is no exact isopycnal mixing scheme, but it serves as an approximation here. For an upper layer grid cell of the square grid where CA has just occurred, the discrctized diffusion scheme reads

$$D_{T^{(1)}} \approx \frac{\kappa_{\mathrm{h}}}{(\Delta x)^2}\left(T^{(2)}(i-1,j) + T^{(2)}(i,j-1) + T^{(2)}(i+1,j) + T^{(2)}(i,j+1) - 4T^{(1)}(i,j)\right) \tag{21}$$

In the grid with hexagonal grid cells, the scheme is computed correspondingly. The diffusion scheme for the lower layer grid point is left unchanged.

The results in Fig. 10 for both the square grid and the grid with hexagonal grid cells show that isopycnal mixing improves the hysteresis curve substantially in our model. There are no such big steps in the curve like in Fig. 1. Only on the steep slope of the curve, some few steps are left (see zoom in Fig. 11), and again, the hexagonal grid exhibits a smoother behaviour.

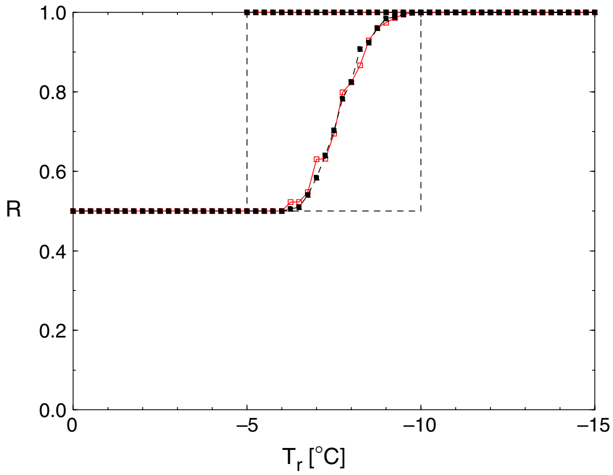

Fig. 10. Hysteresis curves for $R_0 = 0.5$ with the simplified isopycnal mixing scheme. There are only few small steps left. The hexagonal grid (filled squares) performs better than the square grid (empty squares). The zoom is shown in Fig. 11.

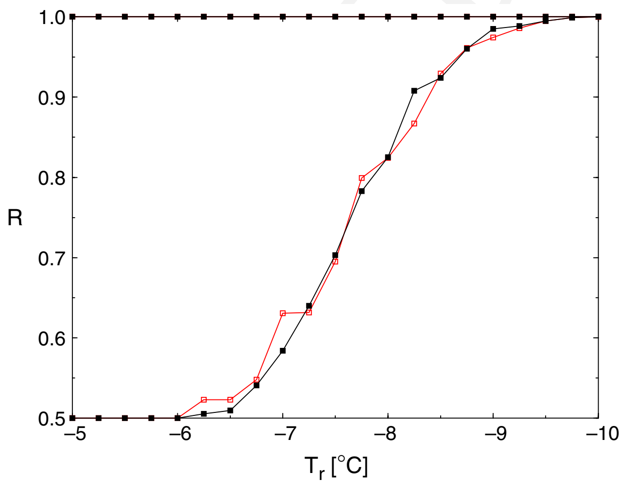

Fig. 11. Hysteresis curves for $R_0 = 0.5$ with the simplified isopycnal mixing scheme. Zoom from Fig. 10. Filled squares represent the hexagonal grid result and empty squares the square grid result.

7. Conclusions

Strongly non-linear, local processes challenge climate modellers in many ways. There is no simple, straight path to avoid the problems that these processes cause in climate models—problems like the difficulties with many parameterizations. One of such local, parameterized processes is ocean convection. Apart from the question which parameterization scheme is optimal, it is not irrelevant for the representation of the dynamics which model grid is chosen. In our study that is based on a conceptual two-layer model, we compare the spreading of convection in a square grid with results obtained using a hexagonal grid.

It turns out that the *local* discretization effect manifests itself in the *average* behaviour of an entire ocean region. This effect is studied in hysteresis experiments in which the surface boundary condition for heat flux is employed as a hysteresis parameter, and the initial convective activity is randomly distributed. The discretization effects are visible as steps in an averaged hysteresis curve. Cessi and Young (1996) have shown the strong sensitivity of the convective adjustment scheme to initial conditions. In this paper, we demonstrate how small scale pattern switches are associated with steps in the hysteresis curve. The first of two major steps is related to direct neighbour cells of convective cells becoming convective, while the second step corresponds to a kind of checkerboard pattern.

Convection in a grid with square grid cells is quite sensitive to the direction of advection. This is an anisotropy which might yield substantial systematic errors in ocean climate models. The errors could be hidden due to the more complex velocity patterns in less idealized velocity fields. The anisotropy is shown here in numerical experiments in which different values for the horizontal angle of a homogeneous velocity field cause clearly different developments of convective activity. Hecht et al. (2000) found a similar result for a test experiment with a horizontal ocean gyre and rotated grids. In their study, it turned out that the representation of the western boundary current depends strongly on a proper and step-free representation of the coastline. Here, the effect of the grid anisotropy is rather surprising, since the lateral boundaries do not affect the results.

A model grid with *hexagonal* instead of square grid cells reduces the height of the steps in the hysteresis curves and significantly improves horizontal isotropy. Even for the—already improved—case with mixing of isopycnal type, the difference between the two grid geometries is recognisable. Such a mixing scheme reduces the discretization effect seen in the hysteresis experiments.

From the restricted viewpoint of these conceptual, numerical experiments, we recommend the hexagonal grid geometry (i.e. icosahedral–hexagonal on the sphere) for ocean climate modelling. For ocean models alone, unstructured grids may be the more useful alternative, since they allow for a better representation of complex orographies. In climate models however, hexagonal grids have another advantage: the flux coupler (between atmosphere and ocean or land surface) in GCMs can be programmed much more efficiently if the icosahedral–hexagonal grid is used in all modules of the model (Randall et al., 2002). If higher resolution was locally needed, this could be done within the framework of hexagonal grid cells (L. Bonaventura, personal communication). Therefore we strongly suggest to perform test experiments with comprehensive ocean models using a icosahedral grid in order to assess the potential value of this grid for ocean climate modelling.

Acknowledgements

TK and ST were supported by the Deutsche Forschungsgemeinschaft (Sfb 555). ST wishes to thank M.A. Morales Maqueda and J. Baehr for useful discussions and M. Thiel for the proofreading. The comments of two anonymous reviewers helped to improve the article.

References

Baumgardner, J.R., Frederickson, P.O., 1985. Icosahedral discretization of the two-sphere. SIAM J. Numer. Anal. 22, 1107–1115.
Braconnot, P., Marti, O., Joussaume, S., 1997. Adjustment and feedbacks in a global coupled ocean–atmosphere model. Clim. Dyn. 13, 507–519.
Cessi, P., 1996. Grid-scale instability of convective-adjustment schemes. J. Mar. Res. 54, 407–420.
Cessi, P., Young, W.R., 1996. Some unexpected consequences of the interaction between convective adjustment and horizontal diffusion. Phys. D 98, 287–300.
Cox, M.D., 1984. A primitive equation, 3-dimensional model of the ocean. Technical Report 1, GFDL Ocean Group. Available from Geophysical Fluid Dynamics Laboratory, P.O. Box 308, Princeton, NJ 08542.
Gent, P.R., McWilliams, J.C., 1990. Isopycnal mixing in ocean circulation models. J. Phys. Oceanogr. 20, 150–155.
Griffies, S.M., Böning, C., Bryan, F.O., Chassignet, E.P., Gerdes, R., Hasumi, H., Hirst, A., Treguier, A.-M., Webb, D., 2000. Developments in ocean climate modeling. Ocean Model. 2, 123–192.
Hecht, M.W., Wingate, B.A., Kassis, P., 2000. A better, more discriminating test problem for ocean tracer transport. Ocean Model. 2, 1–15.
Heikes, R., Randall, D.A., 1995a. Numerical integration of the shallow-water equations on a twisted icosahedral grid. Part I: basic design and results of tests. Mon. Wea. Rev. 123, 1862–1880.
Heikes, R., Randall, D.A., 1995b. Numerical integration of the shallow-water equations on a twisted icosahedral grid. Part II: a detailed description of the grid and an analysis of numerical accuracy. Mon. Wea. Rev. 123, 1881–1887.
Klinger, B.A., Marshall, J., Send, U., 1996. Representation of convective plumes by convective adjustment. J. Geophys. Res. 101, 18175–18182.
Kuhlbrodt, T., Titz, S., Feudel, U., Rahmstorf, S., 2001. A simple model of open ocean convection. Part II: Labrador Sea stability and stochastic forcing. Ocean Dyn. 52, 36–49.
Lenderink, G., Haarsma, R.J., 1994. Variability and multiple equilibria of the thermohaline circulation associated with deep-water formation. J. Phys. Oceanogr. 24, 1480–1493.
Lind, P.G., Titz, S., Kuhlbrodt, T., Corte-Real, J.A., Kurths, J., Gallas, J.A.C., Feudel, U., accepted. Ocean convection modelling studied with coupled bistable maps. Intern. J. Bifurcat. Chaos.
Majewski, D., Liermann, D., Prohl, P., Ritter, B., Buchhold, M., Hanisch, T., Paul, G., Wergen, W., Baumgartner, J., June 2000. The global icosahedral–hexagonal grid point model GME—operational version and high resolution tests. In: ECMWF Workshop on Developments in numerical methods for very high resolution global models. Workshop Proceedings, pp. 47–91.
Marshall, J., Schott, F., 1999. Open-ocean convection: observations, theory and models. Rev. Geophys. 37, 1–64.
Molemaker, M.J., Dijkstra, H.A., 2000. Stability of a cold core eddy in the presence of convection: hydrostatic versus nonhydrostatic modeling. J. Phys. Oceanogr. 30, 475–494.
Ničković, S., Gavrilov, M.B., Tošić, I.A., 2002. Geostrophic adjustment on hexagonal grids. Mon. Wea. Rev. 130, 668–683.
Popović, J.M., Ničković, S., Gavrilov, M.B., 1996. Frequency of quasi-geostrophic modes on hexagonal grids. Metcorol. Atmos. Phys. 58, 41–49.
Rahmstorf, S., 1993. A fast and complete convection scheme for ocean models. Ocean Model. 101, 9–11.
Randall, D.A., Ringler, R.D., Heikes, R.P., Jones, P., Baumgardner, J., 2002. Climate modeling with spherical geodesic grids. Comput. Sci. Eng. (September/October), 32–41.
Ringler, T.D., Heikes, R.P., Randall, D.A., 2000. Modeling the atmospheric general circulation using a spherical geodesic grid: a new class of dynamical cores. Mon. Wea. Rev. 128, 2471–2490.
Ringler, T.D., Randall, D.A., 2002. Potential enthrophy and energy conserving numerical scheme for solution of the shallow-water equations on a geodesic grid. Mon. Wea. Rev. 130, 1397–1410.
Sadourny, R., Arakawa, A., Mintz, Y., 1968. Integration of the nondivergent barotropic vorticity equation with an icosahedral grid for the sphere. Mon. Wea. Rev. 96, 351–356.
Thuburn, J., 1997. A PV-based shallow-water model on a hexagonal–icosahedral grid. Mon. Wea. Rev. 125, 2328–2347.
Titz, S., January 2002. Bifurcations of oceanic overturning and convection in conceptual models of the thermohaline circulation. Ph.D. Thesis, Physics Department, University of Potsdam.

OCEMOD 100
28 August 2003 Type
ARTICLE IN PRESS
No. of Pages 18, DTD = 4.3.1

Tomita, H., Tsugawa, M., Satoh, M., Goto, K., 2001. Shallow water model on a modified icosahedral geodesic grid by using spring dynamics. J. Comput. Phys. 174, 579–613.

Tomita, H., Satoh, M., Goto, K., 2002. An optimization of the icosahedral grid modified by spring dynamics. J. Comput. Phys. 183, 307–331.

Tomita, H., Satoh, M., Goto, K., submitted. Global nonhydrostatic dynamical core on the icosahedral grid, part I: model description and fundamental tests. Mon. Wea. Rev.

Vellinga, M., 1998. Multiple equilibria in ocean models as a side effect of convective adjustment. J. Phys. Oceanogr. 28, 621–633.

Williamson, D.L., 1968. Integration of the barotropic vorticity equation on a spherical geodesic grid. Tellus 20, 642–653.